Supporting Information for

Propagation of Concentration Polarization Affecting Ions Transport in Branching Nanochannel Array

Cheng-Yong Li‡, Zeng-Qiang Wu‡, Chun-Ge Yuan, Kang Wang and Xing-Hua Xia*
‡These authors equally contributed to the work
State Key Laboratory of Analytical Chemistry for Life Science and Collaborative Innovation Center of Chemistry for Life Sciences, School of Chemistry and Chemical Engineering, Nanjing University, Nanjing 210093, China
Fax: (+86) 25 83597436; E-mail: xhxia@nju.edu.cn (X. H. Xia)

Experimental Section

Chemicals and reagents. Aluminum sheets (thickness 0.1 mm; purity 99.99%) were obtained from Xinjiang Zhonghe Limited Corp. (Xinjiang, China). Analytical grade reagents of oxalic acid, sulfuric acid, phosphoric acid, perchloric acid, 36% hydrochloric acid aqueous solution, potassium hydroxide, potassium chloride, stannous chloride, and ethanolwere purchased from Sinopharm Chemical Reagent Co., Ltd. All solutions were prepared daily with deionized water (18.2 MΩ•cm^{-1}, Milli Q). Prior to use, aqueous KCl solutions were all passed through a 0.22 μm filter.

Characterizations. Scanning electron microscopy (SEM) images were acquired on a scanning electron microscope (S-4800 Hitachi, Japan).

Fabrication of branching nanochannels. PAA membranes used in this work were prepared via a two-step aluminum oxidation process (Figure S1).[1] Aluminum sheet was cleaned in acetone and then electrochemically polished with perchloric acid/ethanol (1:9 v/v $HClO_4$:EtOH) at a constant voltage of 10 V for 10 min to achieve mirror finished surface. The temperature of the electrolyte was maintained at 2 ^oC. Anodization process was performed in 0.3 M oxalic acidat 20 °C at a constant voltage of 60 V for 0.5 h. Then, the PAA membrane was etched in an aqueous mixture solution of phosphoric acid (5 wt.%) and chromic acid (1.8 wt.%) at 60 °C to remove the irregular oxide layer formed in the pre-anodization. Subsequently, the first anodization under the same conditions as that in the pre-anodization was performed for 4 h. Upon completion of the first anodization, the barrier layer produced in anodization was thinned by chemically etching in 5 wt.% phosphoric acid at 30 °C for 60 min. The second anodization was carried out at a reduced potential $1/\sqrt{n}$ and the sub-pores were revealed after etching the barrier layer. In our experiments, the PAA membranes consisted with nanochannels I, II and III were anodized at 60 V, 42.5 V and 30V, respectively.

Fabrication of CNTs. The PAA membrane was placed face down in a quartz tubeheated by a tube furnace (Thermo Scientific, Lindberg/Blue M). Polyethylene glycol 2000 in a vessel beneath the PAA membrane provides the main carbon source. Ar flowed through the quartz tube at 200 sccm during the preheating stage. When the

temperature of the furnace reached 600 °C, the flow rate of Ar was decreased to 50 sccm and maintained for 30 min. For visualization, the as-synthesized CNTs/PAA membrane was then dissolved in hydrofluoric acid for 12 h, and the CNTs were collected by centrifugation.

Measurement setup and i-V characterizations. The scheme of ionic current measurement device featuring nanochannels array bridged two electrolytic cells is shown in **Figure S2**. The effective exposure area of nanochannels array was 3.14 mm^2 in the present study. The membrane was clamped between two PDMS films and then placed between two Teflon cells. All ionic current measurements were carried out in the same conductivity bath in a home-made Faraday shielding cage, which has the same ground with all other instruments used. Two Ag/AgCl electrodes were used for applying the trans-membrane potential and measuring the ionic current, since Ag/AgCl electrode is nonpolarizable and very stable. Linear sweep voltammetry was carried out on a CHI 1140 electrochemical workstation (CHI Instrument Co. Ltd., USA). The ionic current through the nanochannel array was measured by scanning the voltage from −1 V to +1 V at a scan rate of 100 mV/s. The pure KCl solution was slightly acidic (pH 6.6) in our conditions due to the dissolution of CO_2 from atmosphere. Its solution pH can be adjusted by either 0.1 M HCl or 0.1 M KOH.

Numerical simulations for ionic transport in PAA membranes with branching nanochannel array. As we mentioned before, the rectification ratio depends critically on surface charge density for all asymmetric geometry nanochannels in our experiments, *i.e.*, the rectification ratio increases with the decrease of branching nanochannels size. In order to understand the observed ion rectification phenomenon, FEM simulations are applied to analyze ion concentration polarization (ICP) in nanochannel with different branching structures. In the case of nanochannels III, 3D numerical model is adopted to precisely simulate the ion transport in multi-branching structure. Considering larger diameter of stem nanochannel (100 nm, it is larger than the thickness of double layer) and higher surface charge, the contribution of electroosmosis should be taken account into the numerical simulation. Therefore, our

simulation properly reflects the actual state of ionic currents in stem-branch nanochannel than Poisson-Nernst-Planck (PNP) equation.[2]

We used the FEM to study the mechanism of ionic current rectification (ICR) in branching nanochannels combining with the PNP equation (eq s1 and eq s2)[3,4] and Navier-Stokes equation (eq s3).

$$\nabla^2\Phi = -\frac{F}{\varepsilon}\sum_i z_i c_i \qquad \textbf{(s1)}$$

$$J_i = -D_i\nabla c_i - \frac{z_i F}{RT} D_i c_i \nabla\Phi \qquad \textbf{(s2)}$$

$$\boldsymbol{u}\nabla\cdot\boldsymbol{u} = \frac{1}{\rho}(-\nabla p + \eta\nabla^2\boldsymbol{u} - F\sum_i z_i\, c_i \nabla\Phi) \qquad \textbf{(s3)}$$

where, J_i ,D_i, c_i, and z_i are the flux, the diffusion coefficient, the concentration, and the charge of species i, respectively; Φ is the electrical potential; ε is the dielectric constant of fluid; u is the electroosmotic flow velocity; ρ is the density of solvent; p is the pressure; F, R and T are the Faraday constant, the ideal gas constant and the Kelvin temperature, respectively.

Based on the above equations, 2D (nanochannels I and II) and 3D (nanochannel III) FEM models are built in the FEM software of COMSOL 3.5a (U.S.A), respectively (**Figures S8, S9 and S10**). We assume that the prepared PAA nanochannels are of uniformed structure and surface properties and the multiple branching is just the change of branching nanochannels diameter. The branching interface is defined as the origin of the cylindrical coordinate (r, z) in 2D simulations. Table S2 summaries the boundary conditions of 2D simulations, where V_a is the electric potential varying against the ground potential at boundary h; σ is the solution pH dependent surface charge density of nanochannels. In our case, the surface charge density varies from +5 to +20 mC/m^2 in solutions with pH lower than the *pI* of alumina and -5 ~ -20 mC/m^2 with solution pH higher than the *pI* of alumina, respectively. The electrolyte of 1 mM KCl is set as the initial concentration in computation domain. The diffusion coefficients of K^+ and Cl^- are 1.957×10^{-9} and 2.032×10^{-9} m^2/s, respectively. Although the 2D nanochannel models can quantitatively describe the ICR effect of nanochannel I, it cannot study the possible cross interference of neighboring nanochannels on the

ion transport in multiple branches in nanochannel III. Especially, the real nature of ion concentration distribution at the branching interfaces, which is crucial to the occurrence of ICR, cannot be described by using the 2D models. Therefore, a 3D simulation model has been used to solve these problems. The 3D model is shown in **Figures S9**. The boundary conditions are similar to the 2D model. The difference is that the line is changed to a face. In the FEM model, we do not consider the transport of H^+ and OH^- because their concentrations are relatively low in our experimental conditions except for solutions with pH=3.0 and pH=11.0 and can be thus neglected . We calculate the ionic current by integrating the ionic flux on the boundary *h* or *a* (eq s4).

$$i = -F\int_s \left(J\left(K^+\right) - J\left(Cl^-\right)\right) \bullet nds \qquad \text{(s4)}$$

In our measurements, the solution pH was adjusted with 0.1 M NaOH or HCl (not buffers) since the charge density of PAA nanochannels will be changed in buffers due to the specific ions adsorption at the surface of nanochannel, especially in PBS. In our previous report, the phosphate anion from the buffer solution will significantly influence the charge density of the PAA.[5] While, K^+ and Cl^- are simple monovalence ions, they do not show specific interactions to the PAA nanochannels. Thus, the charge density of PAA nanochannels could maintain original state in neutral KCl solution. In acidic or basic KCl solution, the charge density of PAA nanochannels will increase due to the protonation or deprotonation of hydroxyl groups on the surface.

In addition, due to overlap of electrical double layer in electrolytes with low KCl concentration, K^+ and H^+ (Cl^- and OH^-) are electrostatically repelled from the positively charged (negatively charged) nanochannel. Therefore, the contribution of H^+ and OH^- to nanochannel conductance is less than the contribution of KCl in the low KCl concentration and the medium range of pH (4-10).

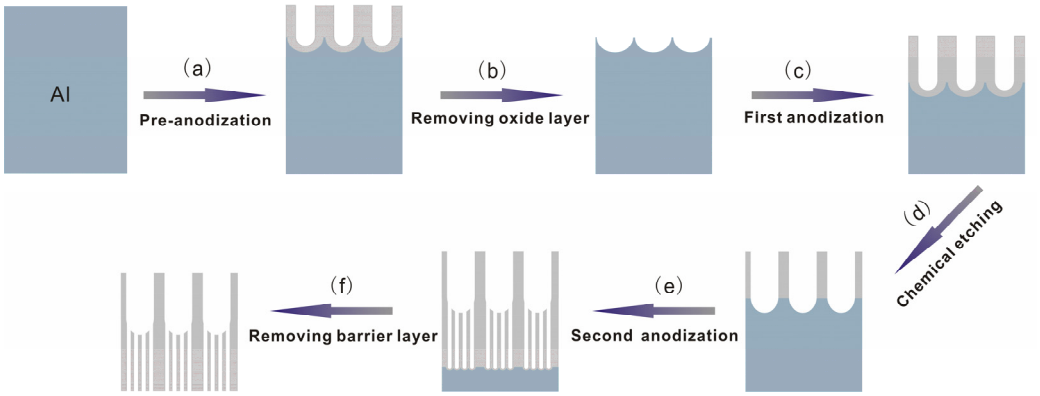

Figure S1. Schematic illustration of the method for fabricating PAA membrane consisting of branching nanochannels.

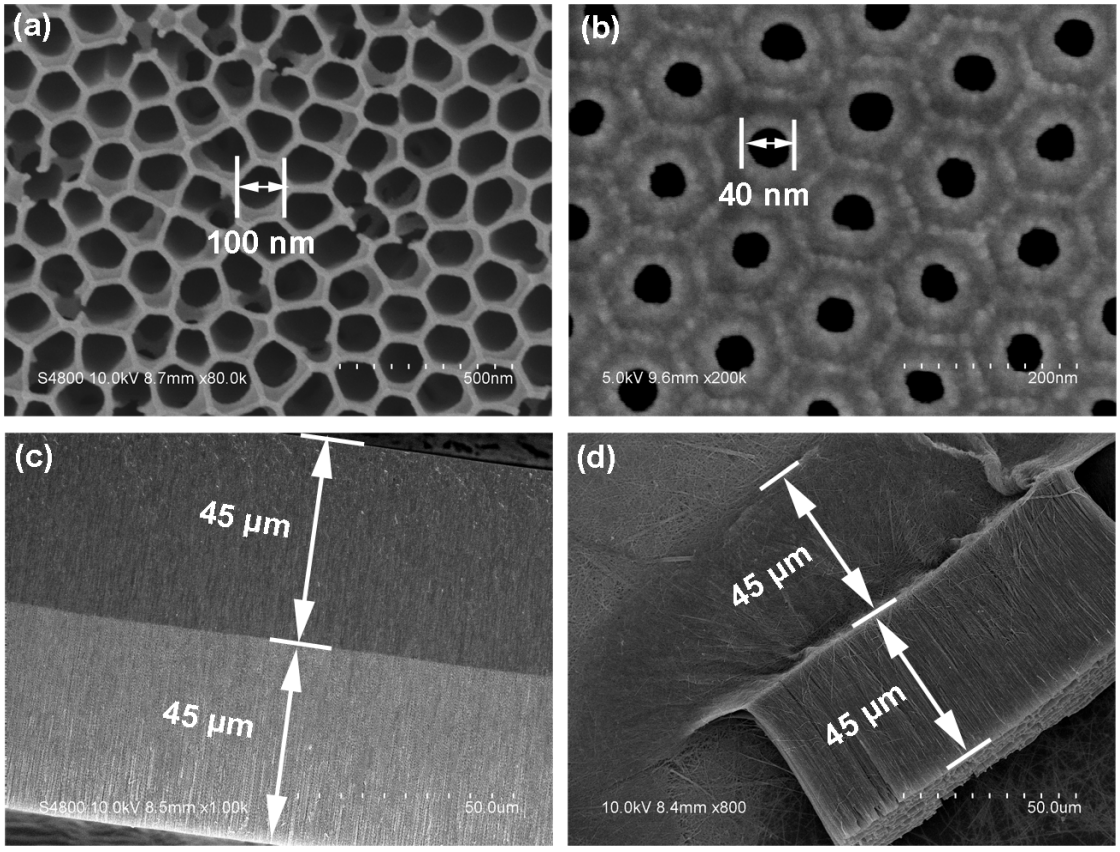

Figure S2. SEM images of the PAA membrane consisting of funnel nanochannels (nanochannel I). The anodization voltage for both steps (c) and (e) was 60 V. a) Top view. b) Bottom view. c) The whole cross-section. d) SEM image of a bundle of CNTs after template removal.

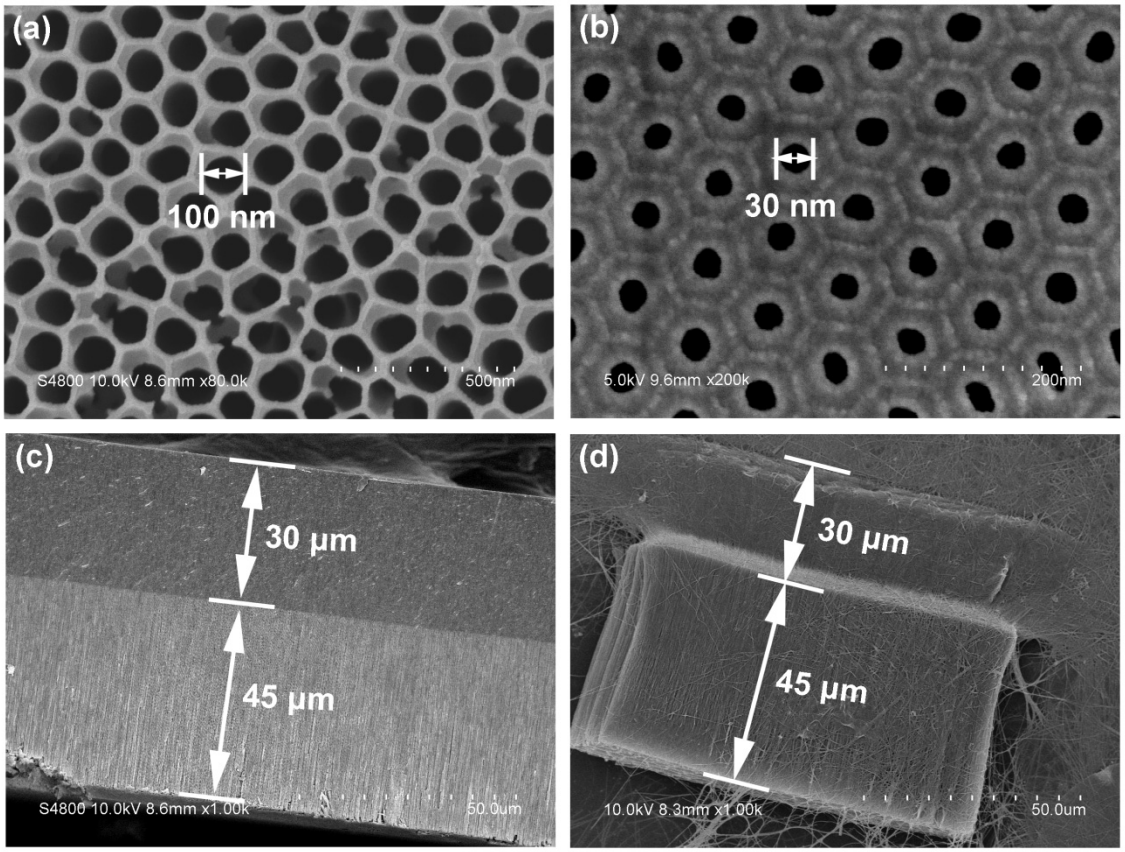

Figure S3. SEM images of the PAA membrane consisting of Y nanochannels (nanochannel II). The anodization voltage for steps (c) and (e) were 60 V and 42.5V, respectively. a) Top view. b) Bottom view. c) The whole cross-section. d) SEM image of a bundle of CNTs after template removal.

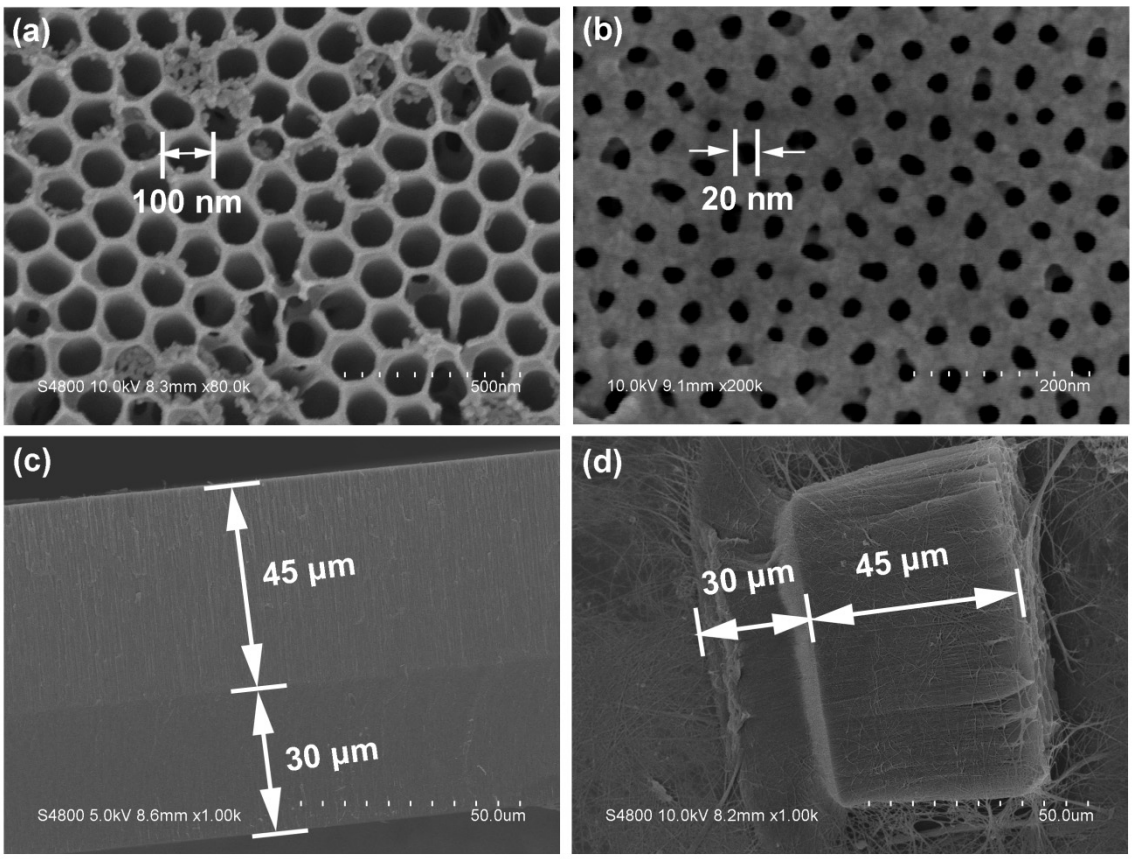

Figure S4. SEM images of the PAA membrane consisting of multiple branching nanochannels (nanochannel III). The anodization voltage for steps (c) and (e) were 60 V and 30 V, respectively. a) Top view. b) Bottom view. c) The whole cross-section. d) SEM image of a bundle of CNTs after template removal.

Table S1. The characteristics of four different nanochannels.

	Stem nanochannels		Branching nanochannels	
	Diameter (nm)	Length (μm)	Diameter (nm)	Length (μm)
Nanochannel I	100±10	45±2	40±5	45±3
Nanochannel II	100±10	45±3	30±3	30±2
Nanochannel III	100±10	45±2	20±5	30±2
control experiment	Diameter =40±5 nm, Length=45±3 μm			

Measured by scanning electron microscope; n=10 for each geometry nanochannels.

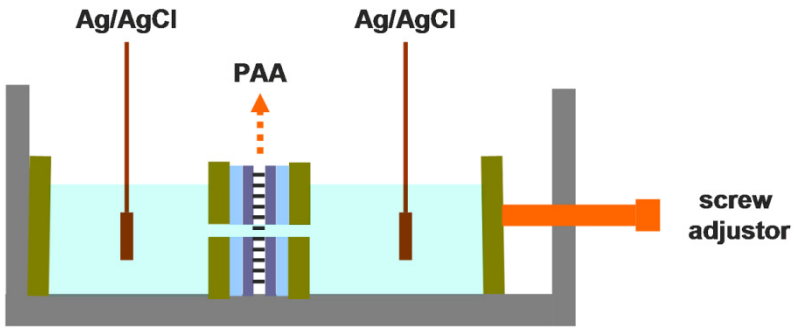

Figure S5. Schematic diagram of *i-V* measurement setup.

Ionic current rectification (ICR) appears when the overlapping of electric double layer (EDL) becomes significant. The thickness of EDL can be approximately predicted by the Debye length λ_D, which depends on the concentration of the ionized fluid, and its thickness λ_D can be estimated by means of the Debye-Hückel parameter *k* (eq. s5).

$$\mathrm{k} = \frac{1}{\lambda_D} = \sqrt{\frac{e^2 \sum_i n_i z_i^2}{\varepsilon \varepsilon_0 k_B T}} \qquad \text{(s5)}$$

where *n, k_B, e, z, T, ε_0* and ε are the concentration, the Boltzmann constant, the electron charge, the valence, the absolute temperature, the dielectric permittivity of vacuum, and the dielectric constant of the solvent, respectively

Ionic current rectification becomes weak at high ionic strength because of the decrease in the thickness of EDL. On the contrary, ion current rectification becomes obvious at low ionic strength as the EDL thickness increasing. We also invesitigated the ionic currents of stem-branch nanochannel with 10 mM KCl solutions at different pH and found that the ionic current rectification is not obvious in 10 mM KCl solution compared with 1 mM KCl solution.

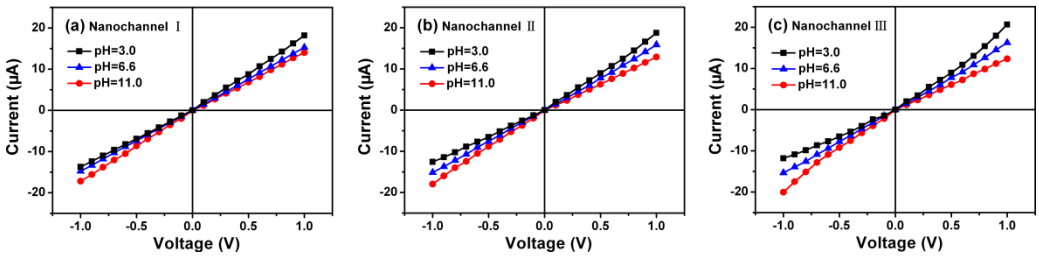

Figure S6. Ionic current characteristics of PAA membranes consisting of different geometry nanochannels measured in 10 mM KCl with different pH values. a) nanochannel I, b) nanochannel II, c) nanochannel III.

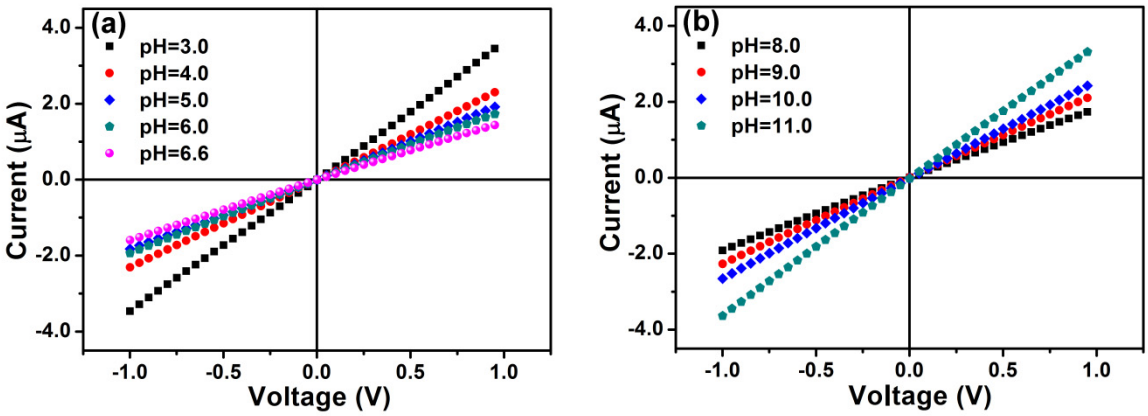

Figure S7. Current-voltage (*i-V*) curves of the PAA membrane consisting of symmetrical non-branching nanochannels in 1 mM KCl with different pH values as indicated in the figures. a) pH 3.0~6.6, b) pH 8.0~11.0. The PAA membrane was anodized at 60 V for both the pre-anodization and the first anodization without chemical etching procedure.

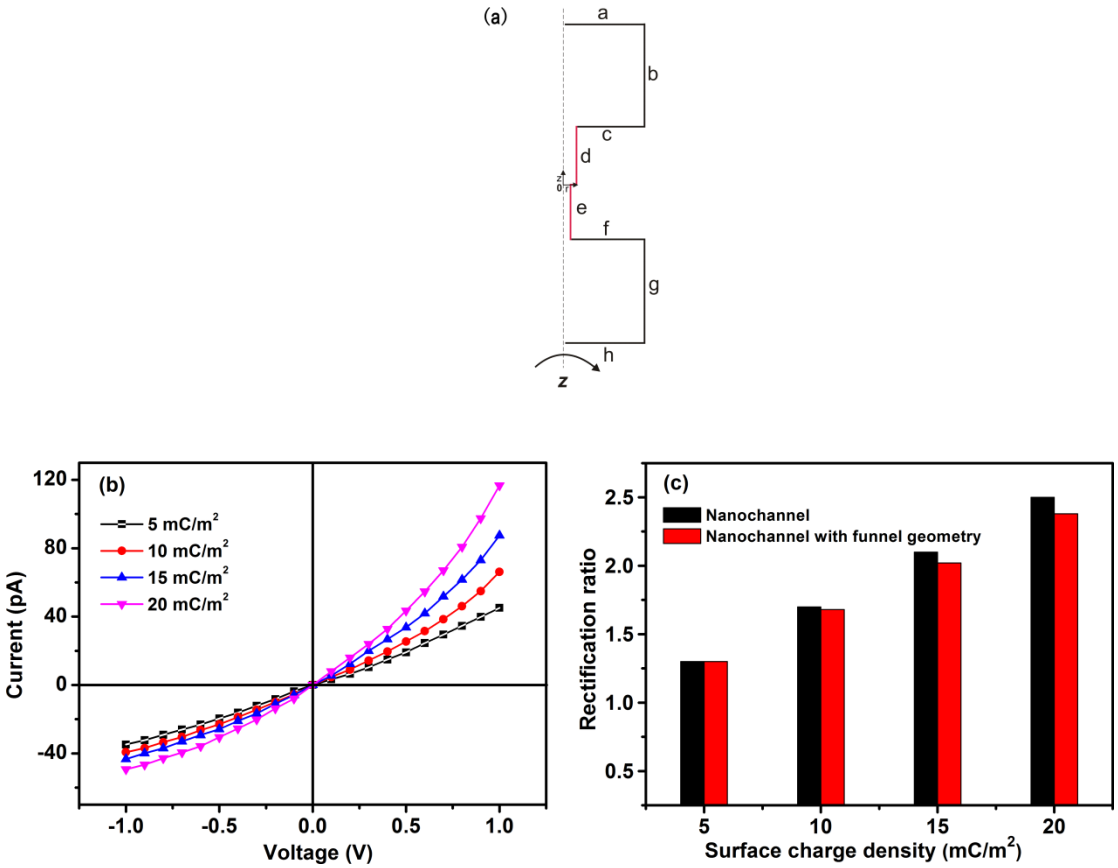

Figure S8. a) Scheme of the 2D computation domain (axis symmetry along z axis) for asymmetric nanochannels (nanochannel I) connected to the two reservoirs. Note that the figure is not drawn to scale. b) The ionic current profiles of PAA nanochannel with funnel geometry versus different surface charge densities. c) Simulated rectification ratio of PAA nanochannel with different geometry. Red color and black color represent the PAA nanochannel with and without funnel geometry, respectively.

The simulated ionic currents and the rectification ratios of PAA nanochannel with funnel geometry are shown in Figure S8. As shown in Figure S8b and S8c, the funnel geometry has less influence on the ICR of PAA nanochannel. As described in our manuscript, the main factor determining the ICR is the concentration distribution regulated by the size and surface charge densities. The funnel geometry will alter the ionic concentration near the connection parts, but it will not change the whole concentration distribution of the nanochannel device.

Table S2. The boundary conditions of the axis symmetry models.

Boundary	Poisson equation (eq s1)	Nernst-Planck equation (eq s2)	Navier-Stokes equations (eq s3)
a	$\Phi = V_a$	$c_1 = c_2 = 1mM$	p=0
h	$\Phi = 0$	$c_1 = c_2 = 1mM$	p=0
b, c, f, g	$n \bullet \nabla\Phi = 0$	$n \bullet J_i = 0$	no slip
d	$n \bullet \nabla\Phi = -\sigma/\varepsilon$	$n \bullet J_i = 0$	no slip
e	$n \bullet \nabla\Phi = -\sigma/\varepsilon$	$n \bullet J_i = 0$	no slip
z	axis symmetry	axis symmetry	axis symmetry

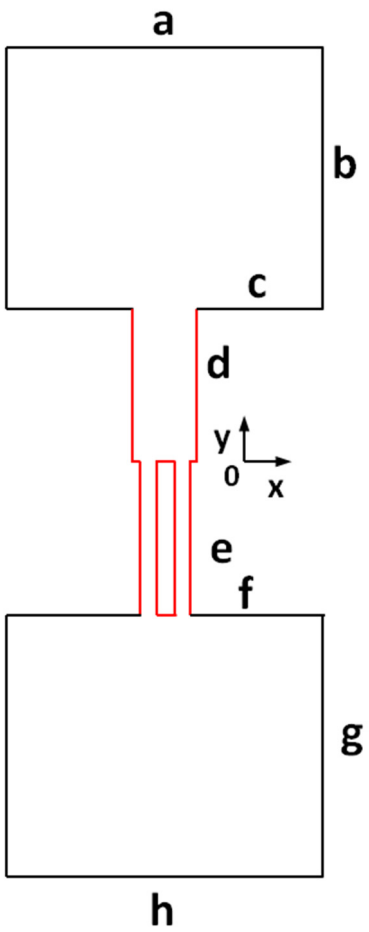

Figure S9. Scheme of the 2D computation domain for nanochannel II connected to the two reservoirs. Note that the figure is not drawn to scale.

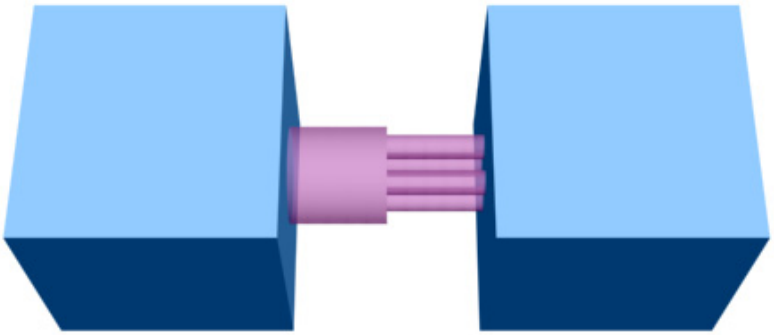

Figure S10. The scheme of the 3D computation domain (nanochannel III) for a charged nanopore (pink) connected to the two reservoirs (blue). Note that the figure is not drawn to scale.

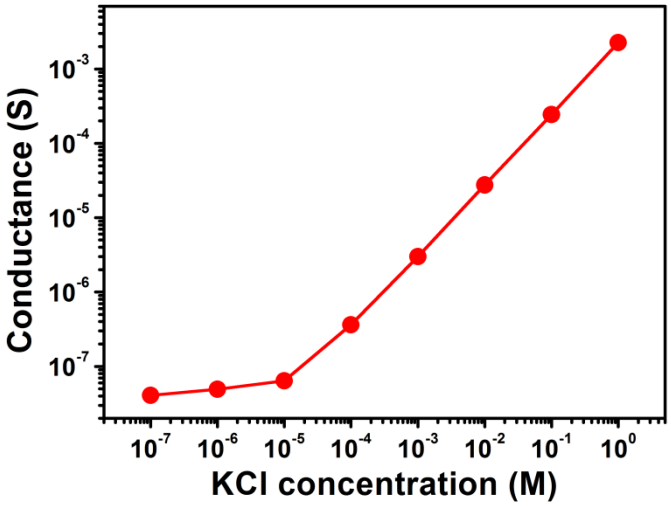

Figure S11. Measured conductance as a function of KCl concentration. The radius and length for this nanochannel are 40 nm and 40 μm, respectively. The porosity of PAA is 6.0×10^9 $(cm^2)^{-1}$. The whole area of PAA is 0.0314 cm^2.

The conductance G of nanochannel for all KCl concentrations can be formulated as sum of the bulk conductance (the first term in right-hand side of eq. s6) and the surface charge governed ions conductance (the second term in right-hand side of eq. s6).[6]

$$G = (\mu_{K^+} + \mu_{Cl^-})cN_A e\frac{\pi r^2}{d} + 2\mu_{K^+}\sigma\frac{r}{d} \qquad \text{(s6)}$$

where μ_{K^+} and μ_{Cl^-} represent the electrophoretic motilities of K^+ and Cl^-, respectively; c is the bulk concentration of KCl; N_A is the Avogadro constant; e is the electron charge; r and d are radius and length of nanochannel, respectively; σ is the effective surface charge density in nanochannel.

As shown in Figure S11, we observe a linear dependence of channel conductance in high concentration region and a conductance plateau in low concentration region. The transition concentration is about 0.5 mM. Therefore, the conductance of nanochannel at low concentration (<0.5 mM) can be ascribed to the surface charge governed ionic transport. By knowing the dimension of nanochannel, the surface charge density (σ) can be derived by fitting the experimental data (eq. s6). Based on the above method, the surface charge density of PAA membrane is about -0.5 mC/m^2 in neutral KCl solution.

However, this method is only suggested to measure the surface charge density of nanochannel in neutral conditions (-0.5 mC/m^2) and cannot be used to investigate the surface charge density of nanochannel in varied pH conditions. Thus, for simulating ionic current rectification of PAA with different pH conditions, we used higher surface densities in FEM simulation considering the protonation or deprotonation of hydroxyl groups on the surface in the acidic or basic solutions.

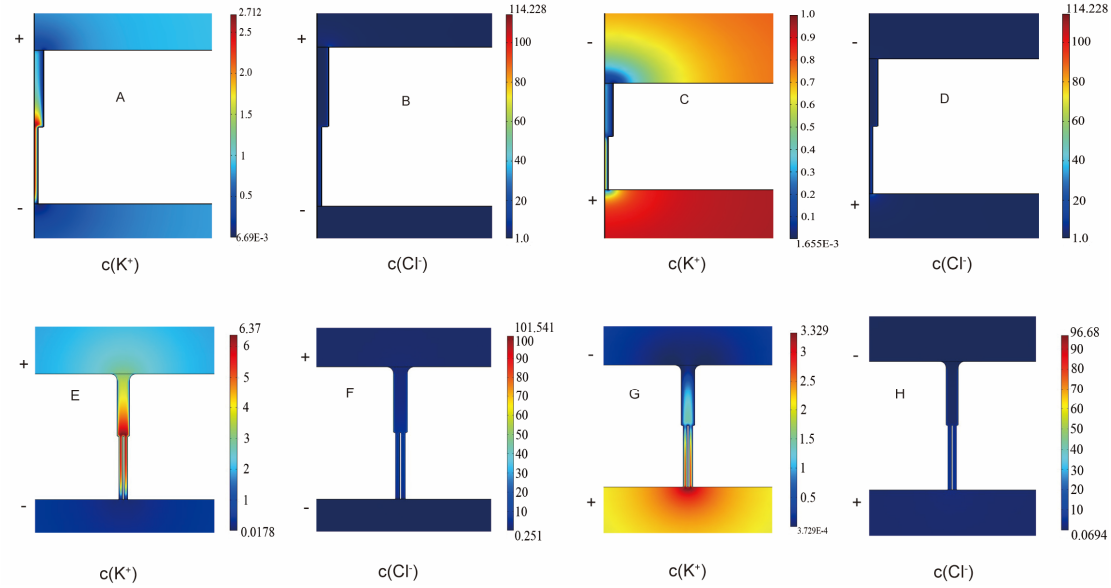

Figure S12. Numerical results of KCl concentration distribution in positively charged nanochannel I and nanochannel II (σ= +15 mC/m^2) with different voltage bias. Figures (A) ~ (D) represent the concentration profiles of K^+ and Cl^- at ± 1 V bias in nanochannel I, respectively. Figures (E)~(H) represent the concentration profiles of K^+ and Cl^- at ± 1 V bias in nanochannel II, respectively. The + and - signs refer to the polarity of the voltage applied across the nanochannel.

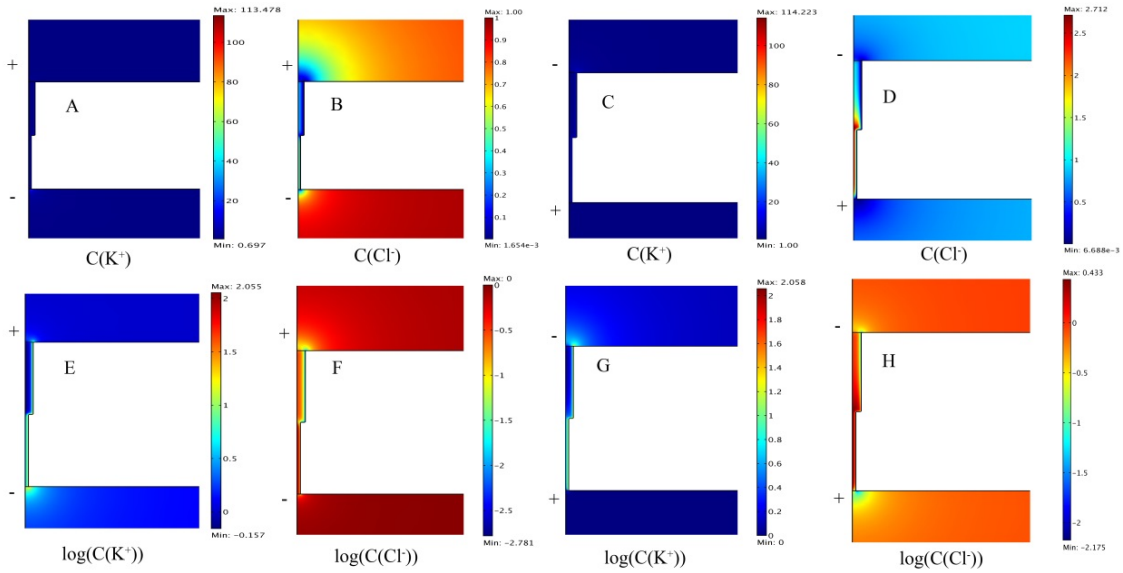

Figure S13. Numerical results of KCl concentration distribution in negatively charged nanochannel I (σ = -15 mC/m^2) with different voltage bias. Figures (A) ~ (D) represent the concentration profiles of K^+ and Cl^- at ±1 V bias in nanochannel I, respectively; Figures (E)~(H) represent the concentration (logarithm coordinate) profiles of K^+ and Cl^- at ±1 V bias in nanochannel I, respectively. The + and - signs refer to the polarity of the voltage applied across the nanochannel.

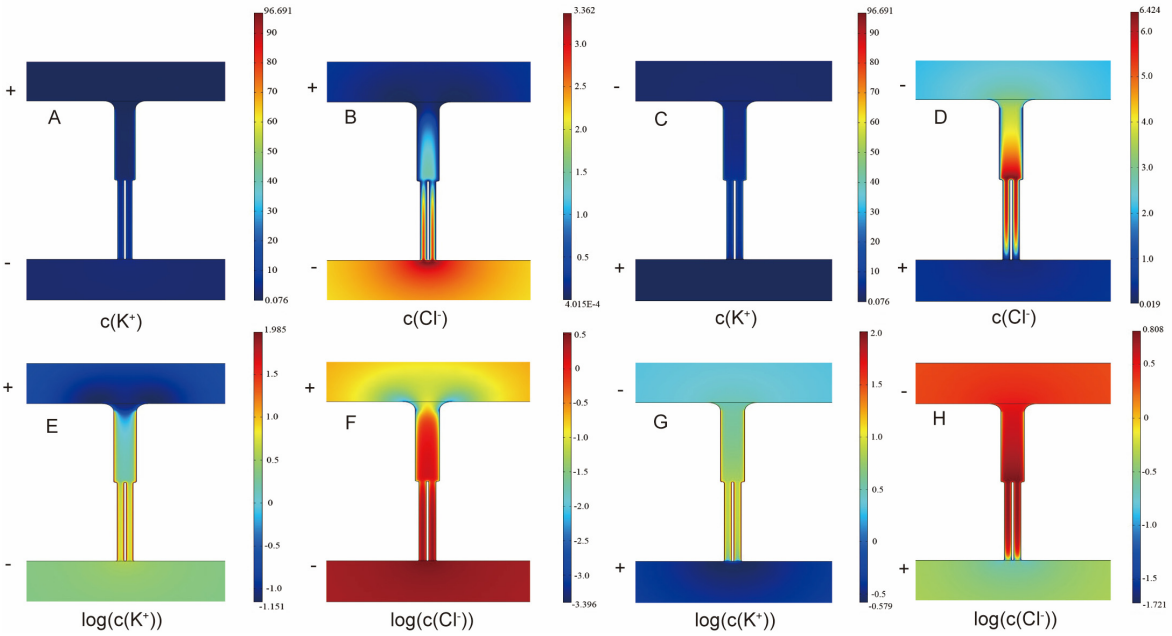

Figure S14. Numerical results of KCl concentration distribution in negatively charged nanochannel II (σ = -15 mC/m^2) with different voltage bias. Figures (A) ~ (D) represent the concentration profiles of K^+ and Cl^- at ±1 V bias, respectively. Figures (E)~(H) represent the concentration (logarithm coordinate) profiles of K^+ and Cl^- at ±1 V bias, respectively. The + and - signs refer to the polarity of the voltage applied across the nanochannel.

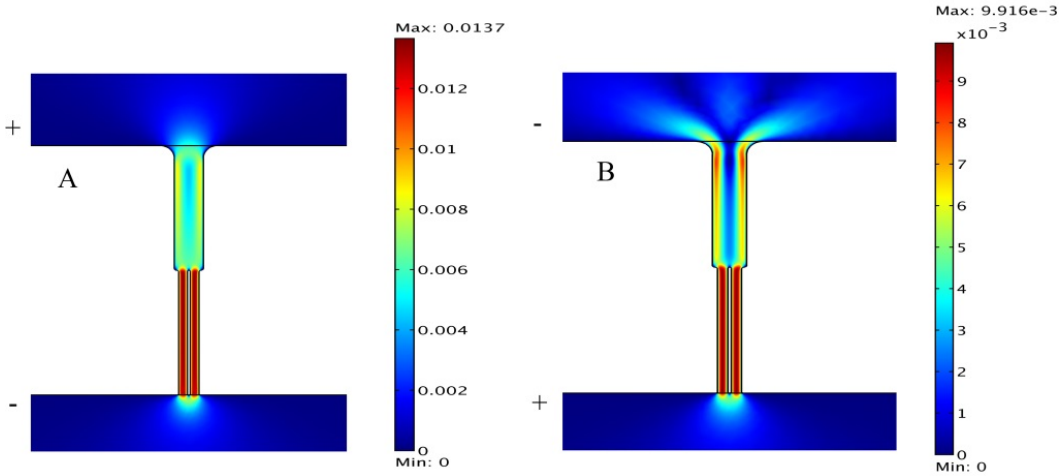

Figure S15. Velocity profiles in positively charged nanochannel II with different voltage bias (A: 1 V, and B: -1 V).

Due to the nanochannel is positively charged, the co-ions are K^+. The electrophoretic mobility of K^+ is 7.62×10^{-8} $m^2\cdot s^{-1}\cdot V^{-1}$.[7] Therefore, the electrophoretic velocity of K^+ at $V_{bias}=\pm1$ V is 0.00191 m/s.

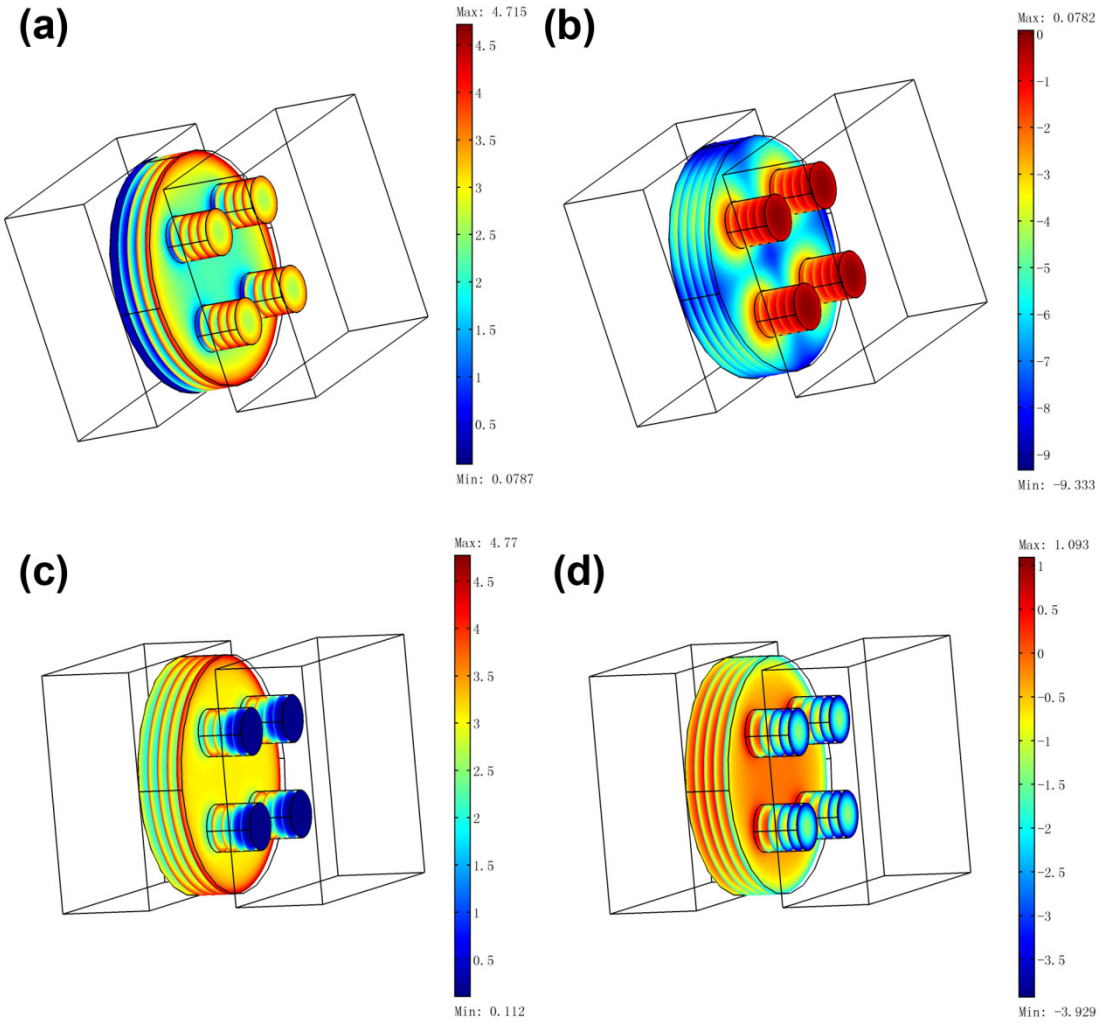

Figure S16. Profiles of the ion concentrations calculated using a 3D model with surface charge σ= -15mC/m^2. a) K^+ concentration at +1 V. b) Cl^- concentration at +1 V. c) K^+ concentration at -1 V. d) Cl^- concentration at -1 V. The bulk KCl concentration is 1 mM. For discriminating between various ions concentrations in nanochannel, the logarithm scale was adopted.

References

(1) Masuda, H.; Fukuda, K. *Science* **1995**, *268*, 1466-1468

(2) Cheng, L.-J.; Guo, L. J. *ACS Nano* **2009**, *3*, 575-584.

(3) Momotenko, D.; Girault, H. H. *J. Am. Chem. Soc.* **2011**, *133*, 14496-14499.

(4) Daiguji, H. *Chem. Soc. Rev.* **2010**, *39*, 901-911.

(5) Chen, W.; Yuan, J. H.; Xia, X. H. *Anal. Chem.* **2005**, *77*, 8102-8108.

(6) Schoch, R. B.; Renaud, P. *Appl. Phys. Lett.* **2005**, *86,* 253111.

(7) Atkins, P.; Paula, J. D., Atkins' Physical Chemistry. 7th editions, 2011.